

An ingenious MMC topology appropriate for motor drives across their entire frequency spectrum

Manoj Dhondiram Patil¹, Mohan P. Thakre², Haridarshan S. Sonawane³, Pawan C. Tapre⁴,
Sunil Somnath Kadlag⁵, Deepak P. Kadam⁶

¹Department of Electrical Engineering, Annasaheb Dange College of Engineering and Technology, Ashta, India

²Department of Electrical Engineering, K. K. Wagh Institute of Engineering Education and Research, Nashik, India

³Department of Energy, Government of State of Maharashtra, Maharashtra, India

⁴Department of Electrical Engineering, SND College of Engineering Education and Research Center, Nashik, India

⁵Department of Electrical Engineering, Amrutvahini College of Engineering, Sangamner, India

⁶Department of Electrical Engineering, MET's Institute of Engineering, Nashik, India

Article Info

Article history:

Received Sep 25, 2022

Revised Dec 19, 2022

Accepted Jan 3, 2023

Keywords:

Energy balance

Field-oriented control

High-frequency mode

Low-frequency mode

Modular multilevel converter

ABSTRACT

Modular multilevel converter (MMC) modules have popped up as among the best choices for medium and high-powered uses. This paper proposes a control scheme for the entire frequency range of operation for the MMC, focusing on supplying a three-phase machine. The machine is required to be controlled in the outer as well as the inner loop. Standard field oriented control (FOC) manages the three-phase machine in the outer closed loop while the inner control has to come up against the problem of energy balancing. That is unevenly distributed and stored in the capacitance of the upper and lower arms of the converter. There are two operating methods used in the inner control loop: a low-frequency method is used for start-up and low-speed operation, and a high-frequency method is for higher speed. In low-frequency mode (LF-mode), a special control strategy has to be implemented to minimize the energy oscillation in the capacitances of the converter arms. It makes utilization of the 3-phase machine's common mode voltage (V_c) as well as internal circulatory currents to verify a symmetrical energy distribution inside this MMC arms and also to avert whatever AC currents inside the DC source.

This is an open access article under the [CC BY-SA](https://creativecommons.org/licenses/by-sa/4.0/) license.



Corresponding Author:

Mohan P. Thakre

Department of Electrical Engineering, K. K. Wagh Institute of Engineering Education and Research

Nashik, Maharashtra, India

Email: mohanthakre@gmail.com

1. INTRODUCTION

The process and control of electrical energy is an essential aspect of power transmission. This task was contented by the conception of power converters such as various levels of multilevel inverters like three-level inverters [1] and five-level inverters [2]. Modular multilevel converter (MMC) has been receiving a lot of attention and advancement ever since its inception because of its numerous advantages such as outstanding performance, high modularity, easy quantification, as well as low voltage and current rating request for switching devices [3], [4]. These would be big benefits of the MMC over conventional two-level as well as configuration converter topologies [5]. The initiation of MMC took place in 2002 for the employment of high-voltage direct current (HVDC) systems in high-voltage transmission implementations [6]. In 2003, Marquardt was the first to present MMC and it turned out to be progressively appealing owing to modularity, high efficiency, excellent V_{out} waveform, redundancy, and avoiding separate dc sources [7]. The first papers

concerning the MMC as a motor drive implementation were publicized in 2009 [8]. Considering the innovation of the MMC, henceforth the topology has been implemented in traction applications [9], HVDC transmission [6], and large electric drives [10], [11], especially for hybrid electric vehicles [12], [13]. This paper is concerned with the behaviour of the HVDC link structured on MMC i.e. dynamic stability. Such articles describe the structure's key principles, the orientation of the inner elements, and thus the management of the MMC. They primarily specialize in a constant frequency operative intent, where almost no special management of levelling the internal energy kept within the cell capacitors has been required. The help managing that has been conferred does not allow function at a low output frequency. Over the years, so many MMC circuit configurations and their computer simulations have been formed, as well as the emergence and technological difficulties of classical and model predictive control techniques have been presented [14]. The first involvement regarding the MMC's low-frequency mode (LF-mode) has been made in [15]. Its basic design has been used in [4] to create an efficient system for MMC low-frequency operation, medium, as well as high voltage applications [16]. It also reduces absorbed current energy and dc fault current [17], [18]. Grid systems and isolated MMC-based DC-DC (IMMDC) inverter help DC buses match voltage, isolation, and transfer power [19]. Such a study elaborates [20]'s strategy for LF-mode associated with the more well-known high-frequency mode (HF-mode). Initially, the management system converts the three- I_{ph} values, as well as the V of the arm capacitance, into space vectors [21] and zero sequence aspects. This technique produces inner energy levelling while preventing any I_{acon} on the DC side. The input, output, as well as inner currents all, can be modified independently using the field oriented control (FOC) [2].

Those who deliver P transfer from DC supply to the motor or in reverse, as well as internal energy transferring here between arms. The real power elements within the converter arms are then assumed for the two operative modes. Sizable V_c variations whenever the machine is running at low speed. So, the extenuating variables i.e. circulating currents and V_{common} mode are used in the low-frequency spectrum to reduce voltage instability [22]. On the flip side, the machine is operated in a high-frequency spectrum when extenuating signals are no longer required. The equations have been derived for the employee during a feed-forward control system to ensure a constant and symmetrical energy transfer. Finally, modelling an MMC with such a time-separate model validated the network [23], [24]. Figure 1 depicts the drive implementation, which includes a DC source, the MMC, and the machine as a 3-ph load. The MMC has been divided into three stages, each with an upper and lower arm n. One converter arm has been made up of m series-connected cells and an inductor. In this arrangement, one cell only needs to be a half-bridge with such a capacitor.

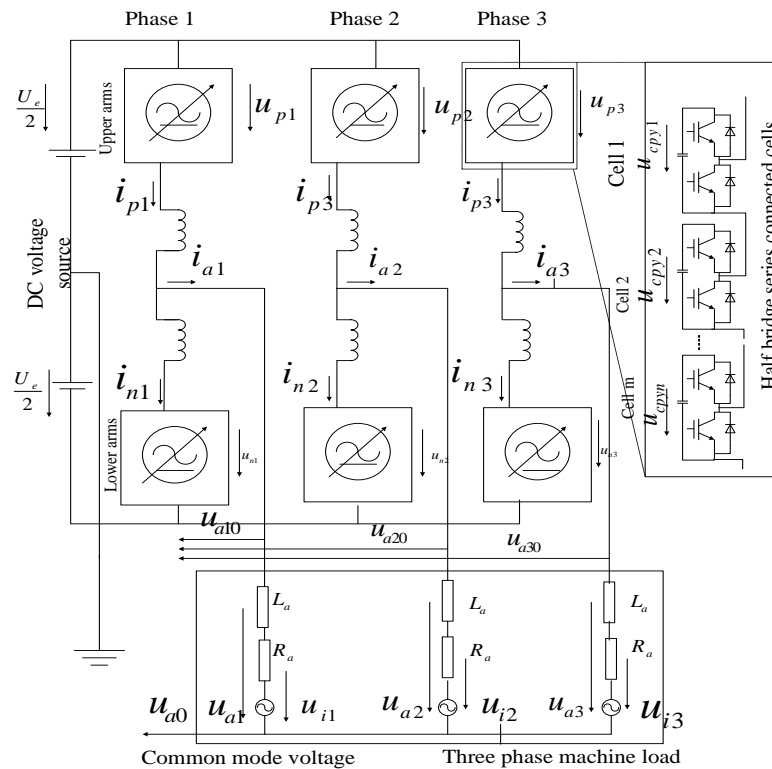


Figure 1. MMC configuration of the 3-phase machine [24]

So, every arm could indeed produce a variable voltage u_{py} and u_{ny} number of phases by switching half-bridges of the cells ($y=1\dots3$). This is same i_{py} and i_{ny} . Currents in the arms have been described. The MMC produces the $3V_{ph}$, $ua10$, $ua20$, and $ua30$ corresponding to a DC source's midpoint 0 on the 3_{ph}-AC side. The V_c mode u_0 also was described as the voltage between the neutral point of the 3-ph load or motor and the DC source's reference potential.

The structure of an article is as follows. Section 1 describes the introduction. Sections 2 provide thorough analysis of motor drive and requirements of variable frequency drive (VFD), motor control with MMC employing current control method is described in section 3. Section 4 discussed recommended method for horizontal (HBC) and vertical balance control (VBC) of MMC with study system modelling and simulation in MATLAB. Section 5 provides and examines the findings of the system simulation of several instances. Finally, article is concluded with the conclusion section 6.

2. MOTOR DRIVE

A motor drive regulates the speed, torque, direction, as well as horsepower produced by a motor. In electro-mechanical drive systems, a VFD regulates AC motor speed and torque by adjusting the input and voltage [25], [26]. The VFD is another technique for regulating the speed of electrical machines. Once users investigate electrical machines or electrical generators, users believe that the speed of rotation of the machines has been governed by the V and f of the stator side of the motor. Modify the torque (1), to alter the speed.

$$T = \frac{K_s E^2 R}{R^2 + (sX)^2} \quad (1)$$

Specifically, T is torque generated by the motor; K_s is constant term; E is rotor EMF induced; R is rotor inductive resistance; X is rotor-induced reactance; and s is slip of the motor.

If a motor torque is less than the load torque, the motor speed has been reduced; if a motor torque exceeds the load torque, the motor speed is increased. Modifying the stator frequency (f) and the number of poles (P) is yet another simple method of controlling the speed of electrical machines [27]-[29]. The rotational speed of a rotating magnetic field has been signified by N_s , which further depend solely on the as well as P . If the P remains unchanged, the only way to change the N_s is to use (2) to modify the f .

$$N_s = \frac{120f}{P} \quad (2)$$

Where N_s is synchronous speed of induction motor, f is stator supply frequency, and P is number of poles of the motor.

On the stator side, parameters such as supply frequency, supply voltage, number of poles, and external stator resistance could be operated to regulate the speed. VFD is an abbreviation for variable-frequency drive, also known as frequency converters that has experienced relatively fast shifts, due primarily to the advancement of a microprocessor as well as semiconducting devices and their cheaper costs. Even so, the fundamental operating precepts of frequency converters stay intact. A VFD has become a type of motor speed controller that controls the frequency and voltage supplied to an induction motor. As shown in the block diagram in Figure 2, a VFD primarily consists of a rectifier, an intermediate circuit, as well an inverter to transform back dc voltage into the ac voltage.

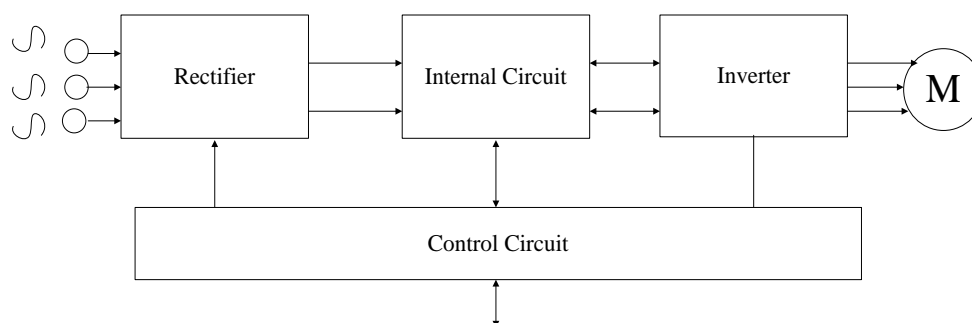


Figure 2. Schematic representation of VFD

Its construction depends on the rectifier and inverter. One transform converted voltage to DC [30], and the other does not. It smoothes the inverter's pulsating direct voltage input. The rectifier converts DC to AC. The

inverter seems to be the final major component of the VFD drive. In addition to generating the output AC voltage and frequency, the inverter process represents the final stage. The ac voltage that is implemented to the motor is generated by the inverter. The frequencies converter's fourth major portion, the control loop, also referred to as the card, controls the semi-conductors, exchanges data with external hardware, assembles and reports problem signals, and protects the converters associated motors. Microprocessors it has enhanced the speed of the controller, growing the variety of applications appropriate for drives as well as reducing the number of estimations required [31], [32]. A processor in microprocessors has been incorporated into the frequency converter and thus can figure out the optimal pulse pattern for each operational state.

3. MOTOR CONTROL WITH THE MMC

Figures 3 and 4 shows the cumulates system model for the MMC and govern mechanisms is shown, that offers the reference attributes for the V_{out} (space vector u_a with a magnitude \hat{U}_a as well as angle γ_a). In this case, a field-or rotor-oriented control serves to completely separately adapt the magnetic flux and torque M_{il} of the machine by i_{ad}^* and i_{aq}^* . In the torque closed loop, a speed controller has been got to add. A zero sequence voltage has been provided in the block "computation of V_{ph} " of Figure 3 and will be discussed clearly.

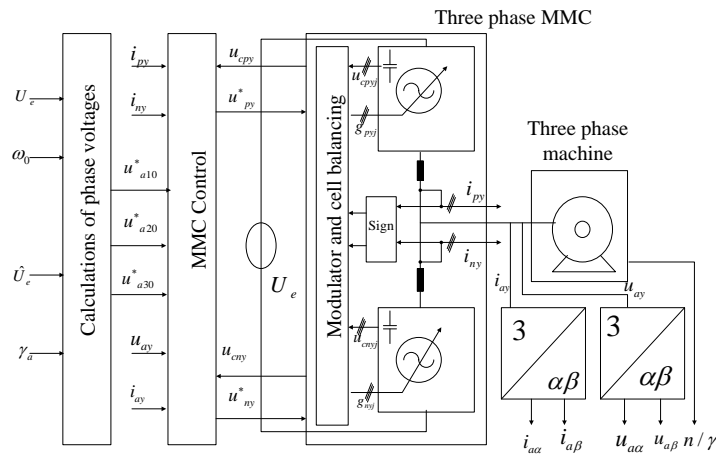


Figure 3. A summary of the MMC-control strategy

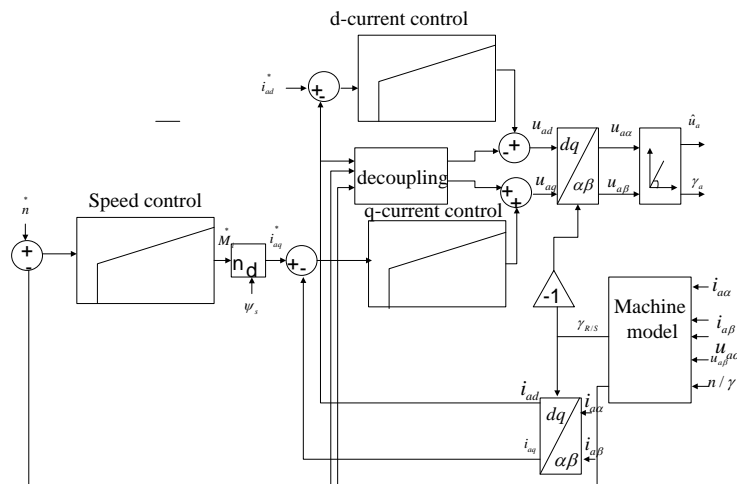


Figure 4. A 3-Ph machine's field/rotor control

The preferred $V_{ph} u_{ay0}^*$ forms the input of the MMC-control block, described in the following sections, along with the measured V and I of the (i_{py} , i_{ny}) and the load (u_{ay} , i_{ay}). The "modulator and cell-balancing" block serves as a link here on its own. It creates the pulse patterns (g_{pxj} , g_{nxj}) for the cell switches

based on the required arm voltages u_{py}^* and u_{ny}^* . [33], [34] define a feasible approach that involves cell balancing. The energy in the arms has been represented by the total amount of the V_C of each arm (u_{Cpy} and u_{Cny}). They are brought back to the MMC-control unit through the modulation scheme.

3.1. Current control

It provides a comprehensive explanation of the decoupled control structure for both i/p and I_o flow [35]. In summary, the $I_o i_{ay}$ has been split in half, and also the $i_{ey}/$ phase flows over the DC-source specified in (3). It thus causes the arm currents:

$$i_{py} = i_{ey} + \frac{i_{ay}}{2}, i_{ny} = i_{ey} - \frac{i_{ay}}{2} \tag{3}$$

$$\Rightarrow i_{ey} = \frac{1}{2}(i_{py} + i_{ny}) \Rightarrow i_{ay} = i_{py} - i_{ny} \tag{4}$$

Independent control of i_{ey} and i_{ay} is possible by adjusting the difference and the sum of the arm voltages given in (4):

$$i_{ay} = \frac{1}{2L\alpha} (u_{ny} - u_{py} - 2(R\alpha * i_{ay} + u_{iy})) \tag{5}$$

$$i_{ey} = \frac{1}{2L} (U_e - (u_{ny} + u_{py})) \tag{6}$$

Its requested arm voltages u_{py}^* , as well as u_{ny}^* , are calculated utilizing voltage loops of every phase provided in (5) and (6) of the MMC. A transition matrix C presently transforms one such strategy in $\alpha\beta 0$ -coordinates to govern the currents seen in Figure 5. The sub-ordinate input current controllers' input signals seem to be the $\alpha\beta 0$ -elements of the current.

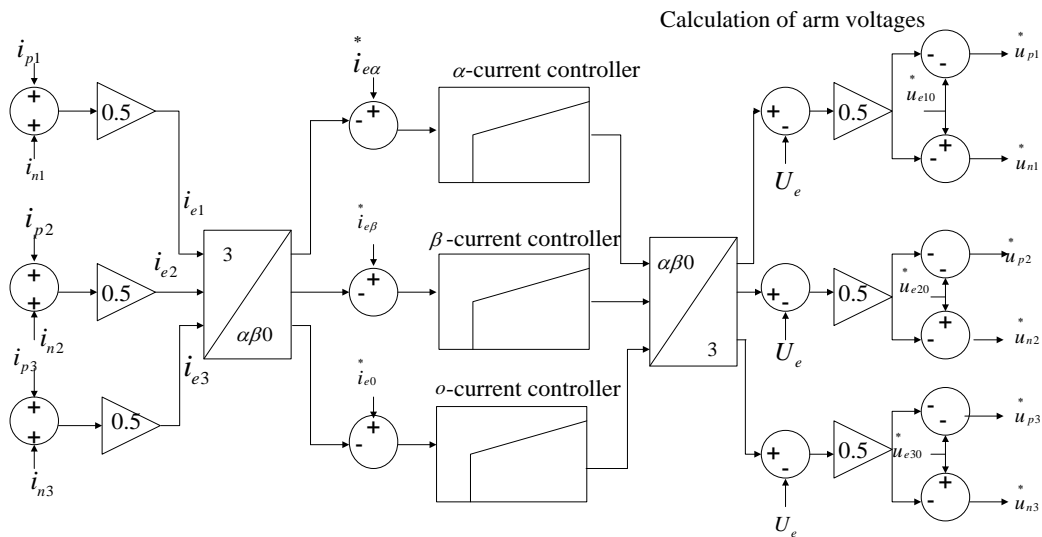


Figure 5. Space current control of the input currents

In Figure 6, the α and β indices are the DC and AC amounts for the internal energy density controller parameters current flow [36] and thus the LF mode feed-forward component (substring v). The 0-component transfers DC energy. DC sources cannot generate I_{ac} because they lack AC signals.

3.2. Functioning mechanisms based on output frequency

Table 1 interprets output V_{ph} depending on the outputting space vector and zero sequence voltages. Identically, the correct output currents inside the phases have been characterized, so although ϕ_a has been the phase difference of the Z_L .

$$i_a = \hat{I}a e^{j(\gamma a - \phi a)} \tag{7}$$

The input currents to further have I_{ey} , \hat{I}_{ey} elements, to the input stage provided by (7) and is employed for energy balance control as in (8).

$$i_{ey} = I_{ey} + \hat{I}_{ey} \cos(\gamma ey) \tag{8}$$

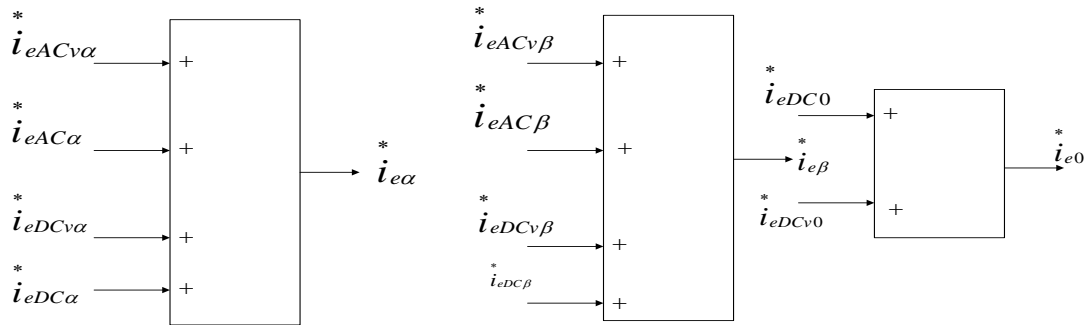


Figure 6. Formation of input current control levels

Name	Voltage
Space vector	$ua = \hat{U}ae^{j\gamma a}$
Phase 1	$ua1 = Ua \cos(\gamma a)$
Phase 2	$ua2 = Ua \cos(\gamma a - \frac{2\pi}{3})$
Phase 3	$ua3 = Ua \cos(\gamma a - \frac{4\pi}{3})$
Zero sequence voltage	$u0 = U0 + \hat{U}0\cos(\omega 0t)$

The arms power must be recognized when acknowledging balance and coordination in both the HF and LF modes:

$$pp_y/n_y = up_y/n_y * ip_y/n_y = (\frac{U_e}{2} \mp u_{ay} \mp u_0) * (I_{ey} + \hat{I}_{ey} \cos(\gamma ey) \pm \frac{i_{ay}}{2}) \tag{9}$$

The real power components for such 2 operating conditions could be calculated using (9).

– HF-mode

In the HF mode, (10) gives a fixed frequency of the V_{out} :

$$\gamma a = \omega at \tag{10}$$

Besides the real power supplies of the input and output sides, a further real power component could be produced by varying the \emptyset of the I_{inner} in (11) γey through relation to the output V_{ph} currents in (11) (Table 2).

$$\gamma ey = \omega at - \frac{2(\gamma-1)\pi}{3} \tag{11}$$

Upper arm	Lower arm	Real P supply
$+\frac{1}{2}U_e I_{ey}$	$+\frac{1}{2}U_e I_{ey}$	Real P_{in}
$-\frac{1}{4}\hat{U}_{ay} I_{ay} \cos(\varphi a)$	$-\frac{1}{4}\hat{U}_{ay} I_{ay} \cos(\varphi a)$	Real P_{out}
$-\frac{1}{2}\hat{U}_{ay} I_{ey}$	$+\frac{1}{2}\hat{U}_{ay} I_{ey}$	Real balancing P

So, the arms have different signs, that element was utilised to balance energies vertically among the upper and lower arms by altering the magnitude \hat{I}_{ey} of an internal current.

– LF-mode

The core concepts of the LF mode have been fully discussed in [5], [6]. The V_o and I_o are presumed to be the DC values provided in (12):

$$\gamma a = \text{Constant} \tag{12}$$

In comparison to an HF mode, the I_{inner} used to balance energy in the arms must correlate to an extra zero sequence AC-voltage $\hat{U}0 \cos(\omega 0t)$. As a result, the \emptyset of the inner currents has been provided in (13):

$$\gamma e y = \omega_0 t \tag{13}$$

The uncontrolled AC- V_c modes frequency has been labelled as ω_0 . Table 3 shows the estimated real power components in the LF mode.

Table 3. Aspects of real P in the arms for LF-mode

Upper arm	Lower arm	Real P supply
$+\frac{1}{2}Ueley$	$+\frac{1}{2}Ueley$	Real P_{in}
$-\frac{1}{2}uayiy$	$-\frac{1}{2}uayiy$	Real P_{out}
$+\frac{1}{4}Ueiy$	$-\frac{1}{4}Ueiy$	Unbalance
$-uayley$	$+uayley +uayley$	caused by DC components
$-\frac{1}{2}\hat{U}0\hat{l}ey$	$+\frac{1}{2}\hat{U}0\hat{l}ey$	Real balancing P
$-U0ley$	$+U0ley$	Additional real power caused by c.m. DC-volt
$-\frac{1}{2}U0iy$	$-\frac{1}{2}U0iy$	

Since the total amount of the real power supplies have to be nil, the I_{dc} for energy transfer from the DC source as well as the magnitude of the AC for inner balance is calculated as shown in (14).

$$Iey = \frac{1}{U_e}(uayiy + U0iy) \tag{14}$$

$$\hat{l}ey = \frac{1}{\hat{U}0}(\frac{1}{2}Ueiy - 2uayley - 2U0ley) \tag{15}$$

Users have been afterward utilized in the LF mode for feed-forward control. Since any I_{ac} must be presented at the DC-source, the total amount of the I_{ac} must be taken into account. The solution to this circumstance has been given in (15). In the LF-m, U_0 acts as feed-forward control for the zero sequence component of vertical balancing.

$$\sum_{y=1}^3 \hat{l}ey = -\frac{3\hat{U}aia}{U_e\hat{U}0}(2U0 \cos(\varphi a) + \frac{1}{2}\hat{U}a \cos(3\gamma a - \varphi a)) \tag{16}$$

$$\Rightarrow U0(\gamma a) = -\frac{1}{2} \frac{\hat{U}a}{\cos(\varphi a)} \cos(3\gamma a - \varphi a) \tag{17}$$

The schematic representation in Figure 7 seems to be the result of (16), and (17) for producing the V_{ph} by introducing the zero sequence.

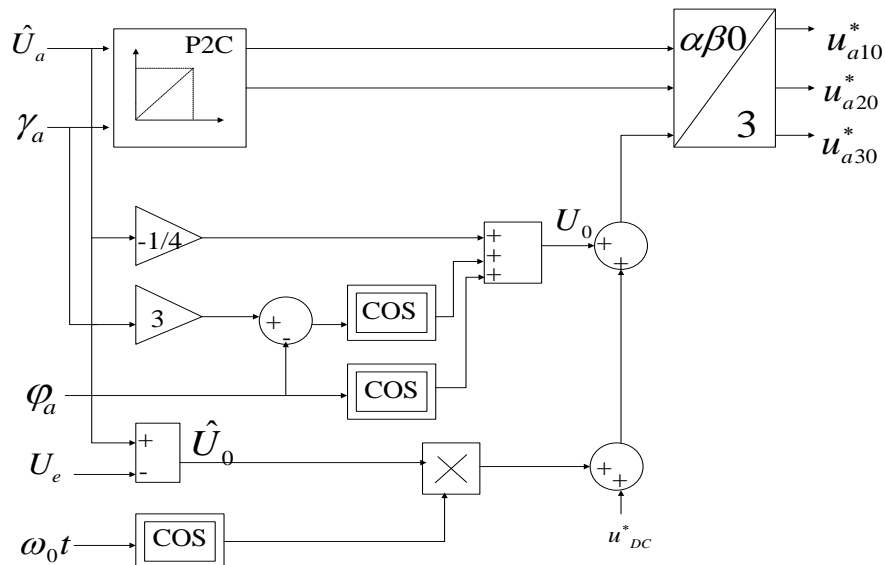


Figure 7. An estimation of the V_{ph} , along with zero sequence voltage

4. PROPOSED METHOD

The strategies introduced for energy balance in the HF as well as LF modes have now been converted into θ - coordinates. One such solution allows the inner energy sources held in the capacitor of each arm across total energy control, along the horizontal axis among MMC's 3-Ph as well as the reference point among arms p and n. The evaluated and converted amplitude of the V_c in the arms must be filtered due to the pulsating energy in the arms.

4.1. Energy control

The output of power/phase has been calculated using the following (18):

$$P_{ay} = \frac{1}{3} \cdot \frac{3}{2} \cdot R e\{u_a \cdot i_a\} = \frac{1}{2} (u_a i_a + u_b i_b) \tag{18}$$

It is employed in the feed forward control of the I_{dc} from the source specified by (19).

$$i_{eDC} v_0 = \frac{P_{ay}}{U_e} \tag{19}$$

An energy controller in Figure 8 adjusts to any changes in normal circumstances as well as maintains the V_{avg} of the arm capacitance at U^*c .

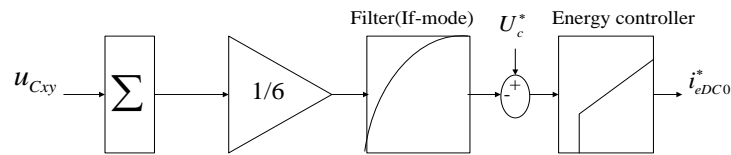


Figure 8. Energy control

4.2. Horizontal and vertical balance control

The govern technique through Figure 9 distributes energy equally among the 3 phases, which are represented by the sum of u_{Cpy} and u_{Cny} . The internal DC-currents in $\alpha\beta$ -elements cancel out the influence change among phase. The VBC in Figure 10 determines the magnitude of the internal currents to confirm that the upper and bottom arms have equivalent average energy entirety. The magnitude of the inner currents $i_{eAC\alpha/\beta/0}$ must be switched over based on the F_o , by the inference of the two operating conditions.

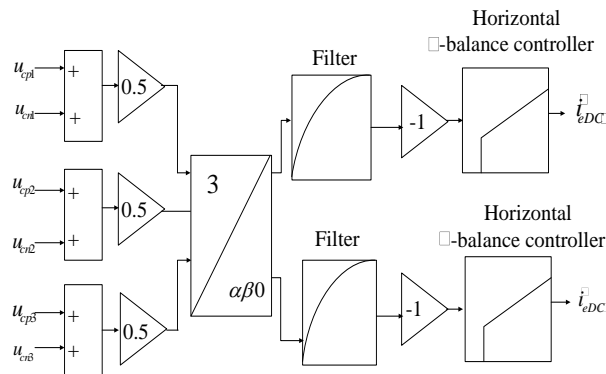


Figure 9. Horizontal balance control

The inner currents must relate to the HF mode's output frequency ω_0 and the LF mode's zero sequence voltage frequency ω_a . A continuous slider shift inside the interval here is between output limits converts the information into HF into LF form ω_{a1} and ω_{a2} . Figure 11 depicts the VBC concept. The magnitude of the inner currents has been magnified by the zero sequence voltage of AC reference curves. These α and β aspects are directed directly to the handover blocks with the necessary internal present value. The extra DC zero sequence influences u^*_{0BCsym} the $\alpha\beta0$ component, which characterizes the distinction between the total the three phases' amount of energy, from highest to lowest.

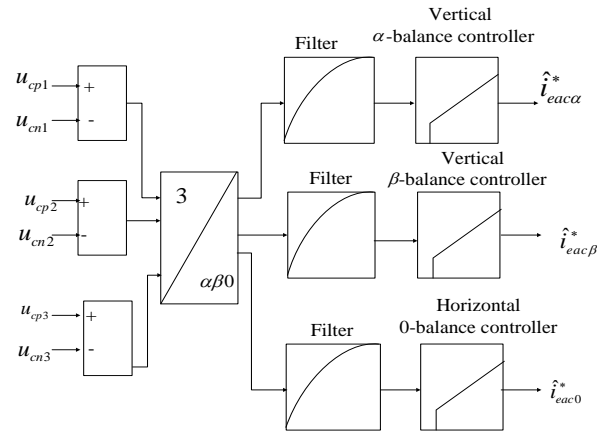


Figure 10. Vertical balance control

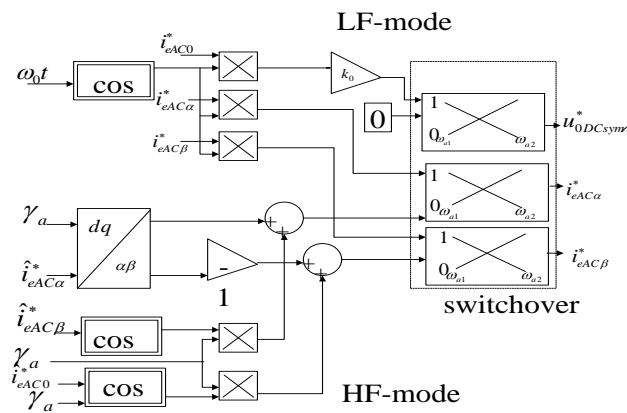


Figure 11. Vertical balancing in the HF and LF modes

Such a technique, as expected, manages to avoid any I_{ac} in the DC_{source} . Having similar objective is accomplished inside the HF mode by using a positive and a negative sequence current mechanism for vertical balances [37]. The feed-forward control currents changed in a similar manner, as shown in Figure 12.

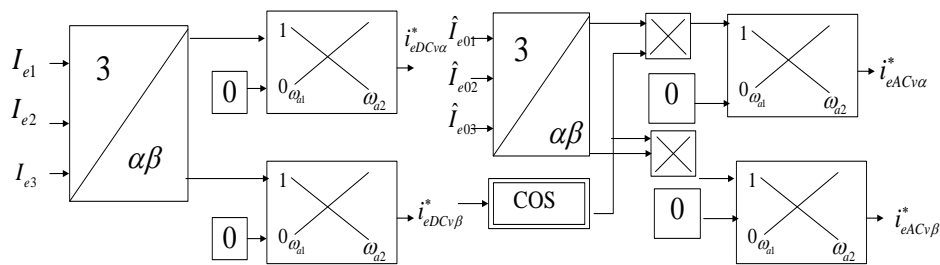


Figure 12. Switchover of the feed-forward balancing control

5. RESULT AND DISCUSSION

Computation in MATLAB surrounding a PLECS block set for such MMC validates the suggested control approach. To ignore the modulator's switching states as well as cancel the ripple currents inside the computation, the arms of the MMCs have been modeled by voltage govern sources. Using given by (20), the voltage of the arm capacitance has been determined step by step.

$$u_{Cxy,k} = u_{Cxy,k-1} + \frac{TA}{c} \cdot \frac{u_{xy,k} \cdot i_{xy,k}}{u_{Cxy,k-1}} \tag{20}$$

3- $\alpha\beta\theta$ -transformation is given by (21):

$$\begin{bmatrix} y\alpha \\ y\beta \\ y0 \end{bmatrix} = C \cdot \begin{bmatrix} x1 \\ x2 \\ x3 \end{bmatrix} = \begin{bmatrix} \frac{2}{3} & \frac{-1}{3} & \frac{-1}{3} \\ 0 & \frac{1}{\sqrt{3}} & \frac{-1}{\sqrt{3}} \\ \frac{1}{3} & \frac{1}{3} & \frac{1}{3} \end{bmatrix} \cdot \begin{bmatrix} x1 \\ x2 \\ x3 \end{bmatrix} \quad (21)$$

Polar-to-Cartesian (P2C) and Cartesian-to-polar (C2P) transformations are depicted by the following (22):

$$\begin{bmatrix} y\alpha \\ y\beta \end{bmatrix} = r \cdot \begin{bmatrix} \cos(\theta) \\ \sin(\theta) \end{bmatrix} \cdot \begin{bmatrix} r \\ \theta \end{bmatrix} = \begin{bmatrix} \sqrt{x\alpha^2 + x\beta^2} \\ \arctan(\frac{x\beta}{x\alpha}) \end{bmatrix} \quad (22)$$

In (23), rotation of the vector by angle γ is given by:

$$\begin{bmatrix} y\alpha \\ y\beta \end{bmatrix} = \begin{bmatrix} \cos(\gamma) & -\sin(\gamma) \\ \sin(\gamma) & \cos(\gamma) \end{bmatrix} \cdot \begin{bmatrix} xd \\ xq \end{bmatrix} \quad (23)$$

Table 4 depicts the specifications of the modeled MMC. A 3- I_{ph} source with the same ($\varphi_0 = 0$) as the V_o space vector could provide the I_o .

Table 4. Computational specifications for MMC

Parameters	Specifications
Sampling time	$T_A=125$ microsec
Input DC voltage	$U_c=100$ V
Arm capacitance	$C=4,400$ microF
Arm capacitance ref. voltage	$U^*_c=120$ V
Zero sequence AC-frequency	$\omega_0=2\pi \cdot 50$ Hz
Switchover frequencies	$\omega\alpha_1 = 2\pi \cdot 15$ Hz, $\omega\alpha_2 = 2\pi \cdot 20$ Hz

Figure 13 illustrates the outcomes of simulating the HF mode. At $t=0.05$ s, the V_{out} will be set to $\hat{U}_a=40$ V, and the output frequency will be set to 40 Hz. The V_{common} mode is display in Figure 14. The DC component of the LF mode that is associated with the 3rd harmonic of the V_c mode is preserved, which allows for the modulation amplitude to be increased. The addition of the V_c is displayed in Figure 15 for each of the six arms, and it is after the step at t is 0.05 s that the efficiency of the inner balancing control can be seen to have been achieved. Figure 16 depicts an illustration of each of the concern 3- Ph input currents. As was to be expected, there is no discernible presence of an AC component in the overall input current denoted by i_e in Figure 17. Figure 18 contains illustrations that illustrate the LF mode.

The extra AC- V_{common} mode is display in Figure 19 seems to be noticeable at the output V_{ph} . An energy pulse inside the capacitor of the arm has been moved to significantly high frequencies, as shown in Figure 20. As a result, the energy pulse, and thus the required C_{arm} , has been drastically decreased. This configuration, depicted in Figures 21 and 22, requires a higher inner AC. In comparison to the HF mode, the total amount of these I_{ac} has always been zero.

High-frequency operation

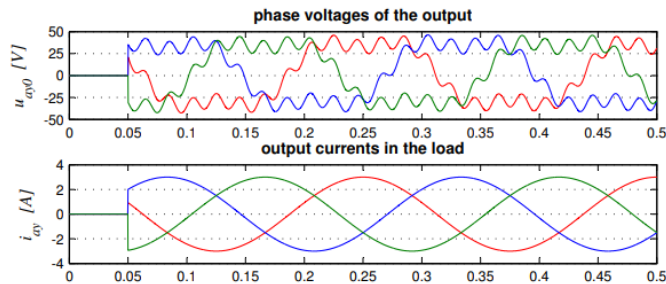


Figure 13. Output phase voltages and currents in the load

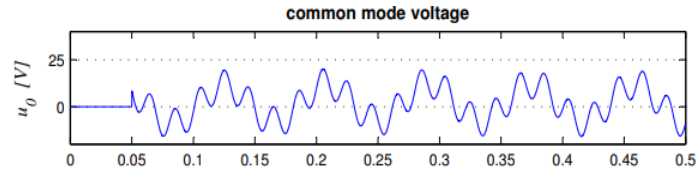


Figure 14. Common mode voltage

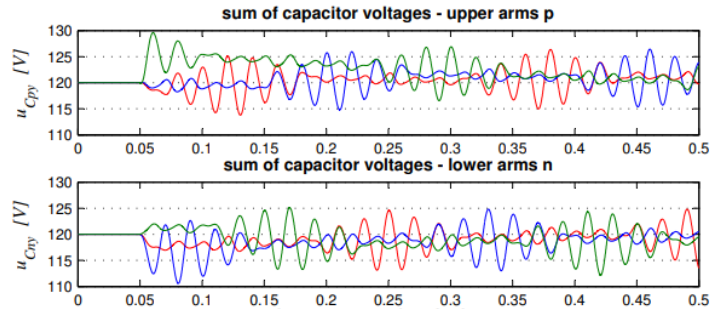


Figure 15. Sum of capacitor voltages

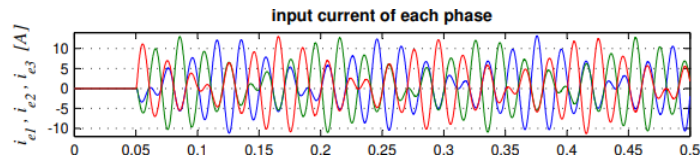


Figure 16. Input current of each phase

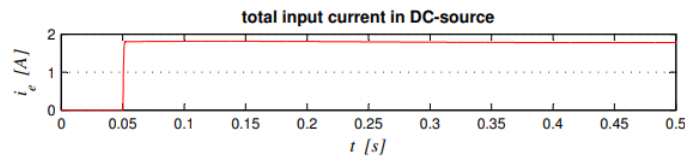


Figure 17. Total input current in DC-source

Low-frequency operation

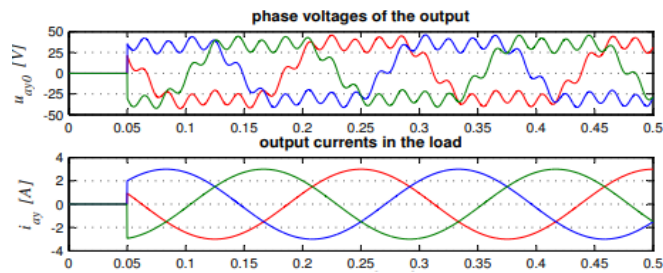


Figure 18. Output Vph and current in the load

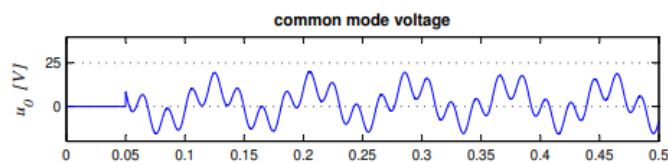


Figure 19. Common mode voltage

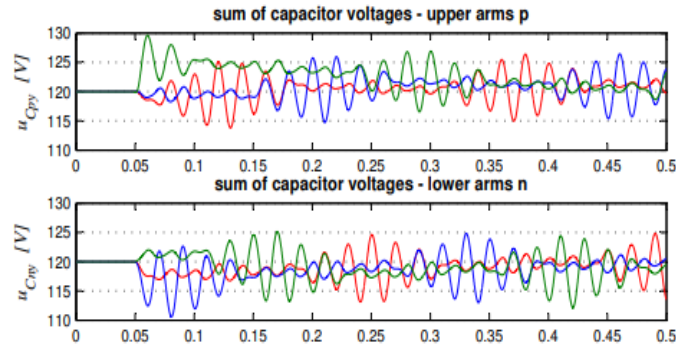


Figure 20. Sum of capacitor voltages

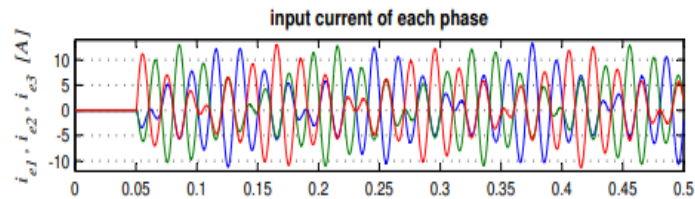


Figure 21. Input current of each phase

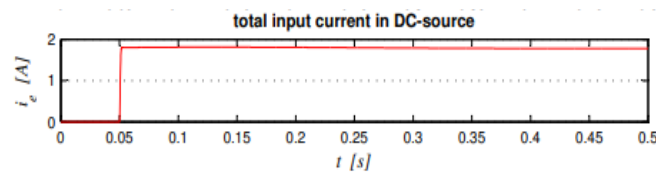
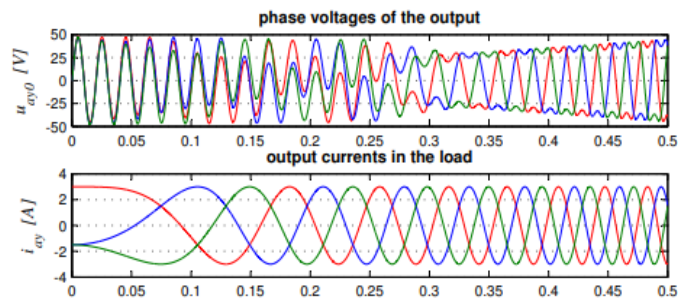


Figure 22. Total input current in DC-source

Figure 23 depicts the transition between the two control techniques. Figure 24 depicts the mode of V of the switchover mode of operation. The frequency and the V_o are risen by $\bar{U}a = 100 \frac{V}{s} t$ and $\omega_0 = 2\pi, 60 \frac{Hz}{s} t$. The change can be observed at time 0.25 s to 0.3 s. Such results indicate a smooth crossover here between LF and HF modes, with very few transients in the V_c of the arms that is shown in Figure 25 than during a hard switchover. Figures 26 and 27 show the input current of every phase as well as the total DC of the source in the switchover operational mode.

Setup of a 3ph system including operation mode

Figure 23. Output V_{ph} and current in the load

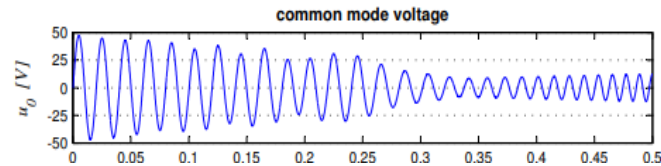
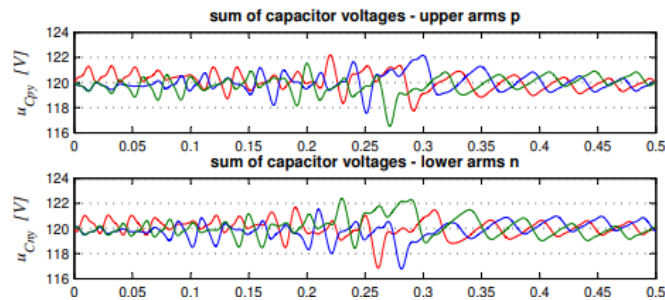
Figure 24. V_c mode

Figure 25. Sum of capacitor Vs

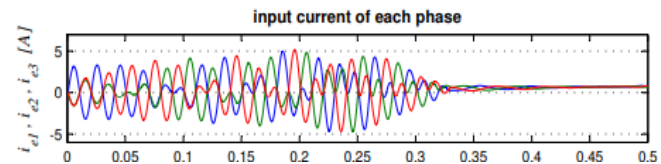


Figure 26. Input current of each phase

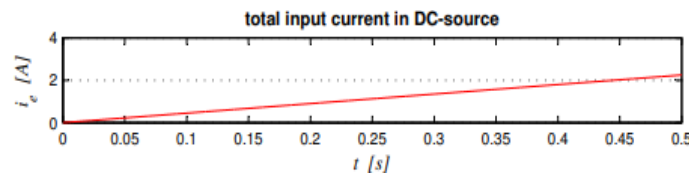


Figure 27. Total input current in DC-source

6. CONCLUSION

It is addressed a coherent approach for regulate the MMC that could produce V_{out} across the entire frequency range of a 3- Ph machine. The contest of balancing V_c throughout all operating conditions has been encountered in this. The remedy has been demonstrated by deriving the decoupled and transmogrified current control on the one hand as well as the real balance of power on the other. The control system has been split into two operation modes: low and high frequency, with separate governs mechanisms. A sliding switchover connects the two strategies. Modeling has been employed to validate this total govern strategy. The findings suggest that the inner balance govern works effectively. The control system ensures that no I_{ac} flow through the DC source at the same time. To conclude, this methodology seems to be capable of controlling an MMC across its entire output frequency range.

REFERENCES

- [1] V. V. Hadke and M. P. Thakre, "Integrated Multilevel Converter Topology for Speed Control of SRM Drive in Plug in-Hybrid Electric Vehicle," in *2019 3rd International Conference on Trends in Electronics and Informatics (ICOEI)*, Apr. 2019, doi: 10.1109/icoei.2019.8862524.
- [2] K. V. Praveenkumar and T. Vinay Kumar, "Space Vector Modulated Direct Torque Control of an Open-end Winding Induction Motor Drive with Three-Level Inversion," *IECON 2021 – 47th Annual Conference of the IEEE Industrial Electronics Society*, 2021, pp. 1-6, doi: 10.1109/IECON48115.2021.9589493.
- [3] A. Dekka, B. Wu, R. L. Fuentes, M. Perez, and N. R. Zargari, "Evolution of Topologies, Modeling, Control Schemes, and Applications of Modular Multilevel Converters," *IEEE Journal of Emerging and Selected Topics in Power Electronics*, vol. 5, no. 4, pp. 1631–1656, Dec. 2017, doi: 10.1109/jestpe.2017.2742938.

- [4] M. N. Raju, J. Sreedevi, R. P. Mandi, and K. S. Meera, "Modular multilevel converters technology: a comprehensive study on its topologies, modelling, control and applications," *IET Power Electronics*, vol. 12, no. 2, pp. 149–169, Feb. 2019, doi: 10.1049/iet-pel.2018.5734.
- [5] J.-S. Lai and F. Z. Peng, "Multilevel converters—a new breed of power converters," *IEEE Transactions on Industry Applications*, vol. 32, no. 3, pp. 509–517, 1996, doi: 10.1109/28.502161.
- [6] L. Chen *et al.*, "Performance Evaluation Approach of Superconducting Fault Current Limiter in MMC-HVDC Transmission System," in *IEEE Transactions on Applied Superconductivity*, vol. 31, no. 8, pp. 1–7, Nov. 2021, Art no. 5602507, doi: 10.1109/TASC.2021.3091045.
- [7] M. Jafari, F. Jafarishadeh, A. Ghasemi, A. Shojaeighadikolaei, S. Saadatmand, and R. Ahmadi, "New MMC-Based Multilevel Converter with Two-And-One Set of Arms and One Inductor," in *2020 IEEE Power and Energy Conference at Illinois (PECI)*, Feb. 2020, doi: 10.1109/peci48348.2020.9064616.
- [8] S. Bernet, "Recent developments of high power converters for industry and traction applications," *IEEE Transactions on Power Electronics*, vol. 15, no. 6, pp. 1102–1117, Nov. 2000, doi: 10.1109/63.892825.
- [9] Y. Li *et al.*, "500 kW Forced Air-Cooled Silicon Carbide (SiC) Three-Phase DC/AC Converter With a Power Density of 1.246 MW/m³ and Efficiency >98.5%," in *IEEE Transactions on Industry Applications*, vol. 57, no. 5, pp. 5013–5027, Sept.–Oct. 2021, doi: 10.1109/TIA.2021.3087546.
- [10] Y. S. Kumar and G. Poddar, "Medium-Voltage Vector Control Induction Motor Drive at Zero Frequency Using Modular Multilevel Converter," *IEEE Transactions on Industrial Electronics*, vol. 65, no. 1, pp. 125–132, Jan. 2018, doi: 10.1109/tie.2017.2721927.
- [11] C. Gan, Q. Sun, J. Wu, W. Kong, C. Shi and Y. Hu, "MMC-Based SRM Drives With Decentralized Battery Energy Storage System for Hybrid Electric Vehicles," in *IEEE Transactions on Power Electronics*, vol. 34, no. 3, pp. 2608–2621, March 2019, doi: 10.1109/TPEL.2018.2846622.
- [12] P. K. Chowdhary and M. P. Thakre, "MMC based SRM Drives for Hybrid EV with Decentralized BESS," in *2020 4th International Conference on Electronics, Communication and Aerospace Technology (ICECA)*, Nov. 2020, doi: 10.1109/iceca49313.2020.9297508.
- [13] M. Kural, F. K. Tuncer, D. Memiş and M. N. Dai, "A Smart Mobility Platform for Electric Vehicles with Event Processing," *2019 IEEE 5th World Forum on Internet of Things (WF-IoT)*, 2019, pp. 480–484, doi: 10.1109/WF-IoT.2019.8767225.
- [14] J. Kolb, F. Kammerer, and M. Braun, "A novel control scheme for low frequency operation of the Modular Multilevel Converter," presented at the PCIM Europe, Nuremberg, Germany, 2011. Accessed: Dec. 27, 2022. [Online]. Available: https://www.eti.kit.edu/english/veroeffentlichungen_1190.php
- [15] A. Lesnicar and R. Marquardt, "An innovative modular multilevel converter topology suitable for a wide power range," in *2003 IEEE Bologna Power Tech Conference Proceedings*, doi: 10.1109/ptc.2003.1304403.
- [16] S. D. Tavakoli, E. Prieto-Araujo, E. Sánchez-Sánchez, and O. Gomis-Bellmunt, "Interaction Assessment and Stability Analysis of the MMC-Based VSC-HVDC Link," *Energies*, vol. 13, no. 8, p. 2075, Apr. 2020, doi: 10.3390/en13082075.
- [17] X. Zhang, X. Kang, and Y. Zhang, "A Strategy of DC Fault Ride Through and capacitor voltage balancing for Hybrid Modular Multilevel Converter (MMC)," in *2019 IEEE 8th International Conference on Advanced Power System Automation and Protection (APAP)*, Oct. 2019, doi: 10.1109/apap47170.2019.9225189.
- [18] M. Thakre, J. Mane, and V. Hadke, "Performance Analysis of SRM Based on Asymmetrical Bridge Converter for Plug-in Hybrid Electric Vehicle," in *2020 International Conference on Power, Energy, Control and Transmission Systems (ICPECTS)*, Dec. 2020, doi: 10.1109/icpects49113.2020.9337059.
- [19] N. Parida and A. Das, "An improved circuit topology of modular multilevel converter (MMC) for DC to AC applications," in *2016 IEEE International Conference on Power Electronics, Drives and Energy Systems (PEDES)*, Dec. 2016, doi: 10.1109/pedes.2016.7914294.
- [20] B. Tai, C. Gao, X. Liu, and Z. Chen, "A Novel Flexible Capacitor Voltage Control Strategy for Variable-Speed Drives With Modular Multilevel Converters," *IEEE Transactions on Power Electronics*, vol. 32, no. 1, pp. 128–141, Jan. 2017, doi: 10.1109/tpe.2016.2535463.
- [21] S. Wang, G. P. Adam, A. M. Massoud, D. Holliday, and B. W. Williams, "Analysis and Assessment of Modular Multilevel Converter Internal Control Schemes," *IEEE Journal of Emerging and Selected Topics in Power Electronics*, vol. 8, no. 1, pp. 697–719, Mar. 2020, doi: 10.1109/jestpe.2019.2899794.
- [22] Z. Zhang, J. Lee, and G. Jang, "Improved Control Strategy of MMC–HVDC to Improve Frequency Support of AC System," *Applied Sciences*, vol. 10, no. 20, p. 7282, Oct. 2020, doi: 10.3390/app10207282.
- [23] J. Zheng, C. Zhang, Y. Cui, X. Kong, Y. Wang and C. Wang, "Accurate Modeling and Fault Analysis of MMC-HVDC System Connected with Offshore Wind Farms," *2021 IEEE Sustainable Power and Energy Conference (ISPEC)*, 2021, pp. 770–774, doi: 10.1109/ISPEC53008.2021.9735990.
- [24] P. Munch, D. Gorges, M. Izak, and S. Liu, "Integrated current control, energy control and energy balancing of Modular Multilevel Converters," in *IECON 2010-36th Annual Conference on IEEE Industrial Electronics Society*, Nov. 2010, doi: 10.1109/iecon.2010.5675185.
- [25] Z. Chang, M. Ma, F. Li, Q. Yang, L. Gao and Z. Lin, "New switched reluctance motor drive with switch capacitor," *8th IET International Conference on Power Electronics, Machines and Drives (PEMD 2016)*, 2016, pp. 1–6, doi: 10.1049/cp.2016.0210.
- [26] A. Shukla, A. Ghosh and A. Joshi, "Flying-Capacitor-Based Chopper Circuit for DC Capacitor Voltage Balancing in Diode-Clamped Multilevel Inverter," in *IEEE Transactions on Industrial Electronics*, vol. 57, no. 7, pp. 2249–2261, July 2010, doi: 10.1109/TIE.2009.2029527.
- [27] R. Breda, M. Biason, S. Calligaro, M. Iurich, S. Mazzer and R. Petrella, "Optimized Distributed Digital Control and Communication Architecture for Flying Capacitor Modular Multilevel Converter Based PMSM Drives," *2022 IEEE Energy Conversion Congress and Exposition (ECCE)*, 2022, pp. 1–8, doi: 10.1109/ECCE50734.2022.9947955.
- [28] S. Das, P. Acharjee and A. Bhattacharya, "Charging Scheduling of Electric Vehicle Incorporating Grid-to-Vehicle and Vehicle-to-Grid Technology Considering in Smart Grid," in *IEEE Transactions on Industry Applications*, vol. 57, no. 2, pp. 1688–1702, March–April 2021, doi: 10.1109/TIA.2020.3041808.
- [29] K. M. S. Y. Konara and M. L. Kolhe, "Charging Coordination of Opportunistic EV Users at Fast Charging Station with Adaptive Charging," *2021 IEEE Transportation Electrification Conference (ITEC-India)*, 2021, pp. 1–6, doi: 10.1109/ITEC-India53713.2021.9932507.
- [30] S. Saravanan, P. U. Rani, and M. P. Thakre, "Evaluation and Improvement of a Transformerless High-Efficiency DC–DC Converter for Renewable Energy Applications Employing a Fuzzy Logic Controller," *MAPAN*, vol. 37, no. 2, pp. 291–310, Jan. 2022, doi: 10.1007/s12647-021-00530-5.

- [31] Z. Geng, M. Han, C. Xia and L. Kou, "A currentless multiple switch open-circuit faults diagnosis strategy for modular multilevel converter with nearest level modulation in HVDC system," in *CSEE Journal of Power and Energy Systems*, doi: 10.17775/CSEEJPES.2021.01710.
- [32] C. S. Phutane, P. K. Katti and G. B. Shinde, "Analysis of Hybrid Energy Storage System for Electric Vehicles," *2022 IEEE 3rd Global Conference for Advancement in Technology (GCAT)*, 2022, pp. 1-6, doi: 10.1109/GCAT55367.2022.9972029.
- [33] H. Mohamed Ismail and S. Kaliyaperumal, "Enhanced Voltage Sorting Algorithm for Balancing the Capacitor Voltage in Modular Multilevel Converter," in *IEEE Access*, vol. 9, pp. 167489-167502, 2021, doi: 10.1109/ACCESS.2021.3134008.
- [34] S. Zhou, M. Guan, B. Li, S. Zhou, and D. Xu, "Control of the hybrid modular multilevel converter in motor drive applications," in *2017 IEEE Applied Power Electronics Conference and Exposition (APEC)*, Mar. 2017, doi: 10.1109/apec.2017.7930765.
- [35] M. A. E. Bolaños, M. Díaz, F. Donoso, A. Letelier, and R. Cárdenas, "Control and operation of the MMC-based drive with reduced capacitor voltage fluctuations," *The Journal of Engineering*, vol. 2019, no. 17, pp. 3618-3623, Apr. 2019, doi: 10.1049/joe.2018.8080.
- [36] Manoj D. Patil, Rutuja V. Nerlekar, Ankita S. Patil, Namrata M. Raut, Ankita M. Virbhakt, "Wireless Charging of Battery in Electrical Vehicle using Solar Energy," *International Journal of Engineering Research & Technology (IJERT)*, vol. 09, no. 03, pp. 394-397, March 2020.
- [37] Z. Liu, K. -J. Li, Z. Guo, J. Wang and J. Qian, "A Comprehensive Study on the Modulation Ratio for Modular Multilevel Converters," in *IEEE Transactions on Industry Applications*, vol. 58, no. 3, pp. 3205-3216, May-June 2022, doi: 10.1109/TIA.2022.3155472.

BIOGRAPHIES OF AUTHORS



Dr. Manoj Dhondiram Patil    was born in Sangli, Maharashtra, India, in 1987. He has received his B.E. degree in Electrical Engineering from Shivaji University Kolhapur, Maharashtra, India in 2009, and the M.E. degree in Electrical Power Systems from Government College of Engineering Aurangabad (which is affiliated with Dr. Babasaheb Ambedkar Marathwada University Aurangabad), Maharashtra, India in 2011, and the Ph.D. degree in Electrical Engineering from Dr. Babasaheb Ambedkar Technological University, Lonere, Raigad, Maharashtra, India in 2020. He is currently working as an Associate Professor at Annasaheb Dange College of Engineering and Technology, Ashta, Sangli, Maharashtra, India. His current research interests include smart grid technologies and multilevel inverters. He can be contacted at email: mdpatileps@gmail.com.



Dr. Mohan P. Thakre    received the B.Tech. and M. Tech degrees in electrical power engineering from Dr. Babasaheb Ambedkar Technological University (Dr. BATU), Maharashtra, India, in 2009 and 2011 respectively, and the Ph.D. degree in electrical engineering from Visvesvaraya National Institute of Technology, (VNIT), Nagpur, Maharashtra, India in 2017. Currently, he is an Assistant Professor at the Department of Electrical Engineering, K. K. Wagh Institute of Engineering Education and Research, Nashik, India. His research interests include flexible AC transmission systems (FACTS) and power system protection. He can be contacted at email: mohanthakre@gmail.com.



Haridarshan S. Sonawane    is working as an Assistant Electrical Inspector in the Electrical Inspectorate wing of the Government of State of Maharashtra, India. He is in service to Government since 2012. He graduated his engineering with a first-class B.Tech degree in Electrical from Government College of Engineering, Pune, and Maharashtra, India in 2010. He received a Master's degree in Power System (Electrical), from the University of Pune, Maharashtra, India. His research interests are in the areas of transmission line protection and renewable energy. He can be contacted at email: haridarshanss@gmail.com.



Dr. Pawan C. Tapre    received the B.E. and M.E. degrees in Electrical Power System Engineering from Sant Gadge Baba Amravati University (SGBAU), Maharashtra, India, in 1995 and 2002 respectively, and a Ph.D. degree in Electrical Engineering from Dr. C.V. Raman University (Dr. CVRU), Bilaspur, Chhattisgarh, India in 2022. Currently, he is an Assistant Professor at the Department of Electrical Engineering, S.N.D. College of Engineering and Research Center, Yeola (Nashik), Maharashtra, India. His research interests include deregulated power systems, flexible AC transmission systems (FACTS), power systems, and power system protection. He can be contacted at email: pawan.tapre73@gmail.com.



Dr. Sunil Somnath Kadlag    did B.E in Electrical Engineering from Dr. Babasaheb Ambedkar, Marathawada University, Aurangabad (Dr. B.A.M.U) in 1997 and an M.E in Electrical Engineering (control system) from Government College of Engineering Pune (Pune University) in 2005. He had done a Ph. D in Electrical Engineering from Suresh Gyan Vihar University Jaipur (Rajasthan) in 2021. His research area is electric vehicles. He is presently working as an Associate Professor and Head, of the Department of Electrical Engineering, Amrutvahini College of Engineering, Sangamner, Savitribai Phule Pune University, Pune, Maharashtra, India. He can be contacted at email sunilkadlag5675@gmail.com.



Dr. Deepak P. Kadam    received a B.E from the Government College of Engineering, Amaravati, and M.E degrees in electrical power systems from Walchand College of Engineering, Sangli, Maharashtra, India, in 1997 and 2005 respectively, and the Ph.D. degree in electrical engineering from Savitribai Phule Pune University, Pune Maharashtra, India in 2015. Currently, he is an Associate Professor at the Department of Electrical Engineering, Bhujbal Knowledge City, MET Institute of Engineering, Nashik, India. His research interests include renewable energy technology, power quality, and power system. His total teaching experience is around 23 years. He can be contacted at email: dpkadam@gmail.com.